Soil Moisture Scatter Radio Networking with Low Power

Spyridon-Nektarios Daskalakis, *Student Member, IEEE*, Stylianos D. Assimonis, Eleftherios Kampianakis, *Student Member, IEEE*, and Aggelos Bletsas, *Senior Member, IEEE*

A low-cost (6 Euro per sensor), low-power (in the order of 200 μW per sensor), with high communication range (in the order of 250 meter), scatter radio sensor network is presented, for soil moisture monitoring at multiple locations. The proposed network utilizes analog frequency modulation (FM) in a bistatic network architecture (i.e., the emitter and reader are not co-located), while the sensors operate simultaneously, using frequency division multiple access (FDMA). In contrast to prior art, this work utilizes an ultra-low cost software-defined radio reader, offers custom microstrip capacitive sensing with simple calibration, as well as modulation pulses for each scatter radio sensor with 50% duty cycle; the latter is necessary for scalable network designs. Overall root mean squared error (RMSE) below 1% is observed, even for ranges of 250 m. This is another small (but concrete) step for the adoption of scatter radio technology as a key enabling technology for scalable, large-scale, low-power and cost environmental sensor networking.

Index Terms—**Scatter radio, sensor networks, soil moisture.**

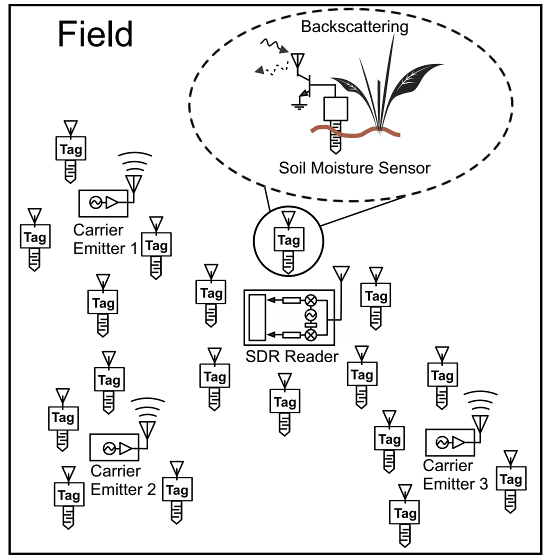

Fig. 1. Bistatic soil moisture scatter radio WSN. There could be multiple carrier emitters and one software-defined radio (SDR) reader.

I. Introduction

MODERN agriculture applications necessitate cheap, effective, low-maintenance and low-cost wireless telemetry for various environmental parameters [1], such as environmental humidity, soil moisture, barometric pressure and temperature [2]–[5]. Continuous and dense environmental monitoring is critical for optimal crop and water management techniques and thus, wireless sensor network (WSN) technologies for microclimate monitoring in extended areas, are indispensable within this topic [1]. One important environmental variable that needs careful monitoring, especially in agriculture and water management applications, is percentage soil moisture ($\%$SM). Prior art has offered novel soil moisture capacitive sensors integrated with discrete wireless radio module [6], [7] or discrete processing chip [8], including ink-jet fabrication designs.

Conventional WSNs consist of a network of nodes (possibly in a mesh architecture), transferring monitored environmental data to a base station. Each node typically employs a Marconi-type radio, controlled by a microcontroller unit (MCU) and the sensors. However, large-scale deployments of conventional WSN technology are uncommon, due to power consumption, installation and maintenance cost. Work in [9] is one rare case of large-scale, outdoor demonstration, with packaging/long-term deployment cost per wireless sensor in the order of 50 Euro.

In order to address power consumption and cost per sensor constraints, scatter radio has recently attracted interest for wireless sensing development (Fig. 1); using scatter radio, the front end of each sensor is simplified to a reflector that modulates information on the sensor's antenna-load reflection coefficient; in scatter radio, communication is performed by means of reflection, where signal conditioning such as filtering, mixing or amplification at the sensor/tag are typically avoided; in that way, low power consumption is needed, offering opportunities for battery-less operation [10], [11], e.g., each sensor can be powered using ambient radio frequency (RF) energy with appropriate rectifiers (e.g., [12]–[14]) or using multiple kinds of ambient energy sources, such as RF and solar energy, simultaneously (e.g., [15]). Sensor designs with scatter radio typically exploit variations of sensor's antenna properties [16], based on the environmental parameter under monitoring, such as the (mechanical) shape (e.g., [17]) or the dielectric constant (e.g., [18]); chip-less designs typically include appropriately-designed antenna loads

This work was supported by the ERC04-BLASE project, executed in the context of the "Education & Lifelong Learning" Operational Program of the National Strategic Reference Framework (NSRF), General Secretariat for Research & Technology (GSRT), funded through European Union-European Social Fund and Greek national funds. It was also supported by an Onassis Foundation graduate studies 2015/16 scholarship.

S.-N. Daskalakis and A. Bletsas are with the School of Electronic and Computer Engineering (ECE), Technical University of Crete (TUC), GR-73100 Chania, Greece (e-mail: sdaskalakis@isc.tuc.gr; aggelos@telecom.tuc.gr). S. D. Assimonis was with ECE TUC. He is now with the School of Electronics, Electrical Engineering and Computer Science, Queen's University Belfast, Belfast BT7 1NN U.K. (e-mail: s.assimonis@qub.ac.uk). E. Kampianakis was with ECE TUC. He is now with Department of Electrical and Computer Engineering, University of Washington, Seattle, USA, 98195. (e-mail: ekampian@washington.edu).

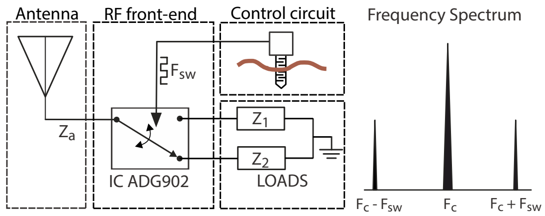

Fig. 2. Scatter radio principles: The low power RF switch "ADG902" alternates the termination loads Z_1 and Z_2 of the antenna (corresponding to reflection coefficients Γ_1, Γ_2, respectively) with frequency F_{sw}. When the illuminating carrier frequency is F_{c}, two new subcarrier frequencies $F_{\text{c}} \pm F_{\text{sw}}$ appear in the spectrum. Difference $|\Gamma_1 - \Gamma_2|$ should be maximized; however, practical constraints (e.g., parasitics) restrict such maximization.

with delay lines (e.g., work in [19] and references therein); another way to construct scatter radio signal reflectors is by using a switch, connecting sensor's antenna to different loads. Elevating the above principles from sensing to networking of several, simultaneously operating, scatter radio sensors is not trivial and emerges as a challenging topic of research.

Work in [20] offered frequency-modulated scatter radio signals with soil moisture information and duty-cycled operation that reduced the operating bandwidth, while experimental results were reported for only two sensors and commodity software defined radio (with cost in the order of 1000 Euro). The tag-to-reader communication range was in the order of 100 meter. In this work, 50% duty-cycle of frequency modulated soil moisture is achieved with a new circuit, which also reduces the overall power consumption; 50% duty cycle is crucial for getting rid of even-order harmonics and thus, enhancing the available bandwidth for multiple scatter radio sensors simultaneous access [21]. Moreover, this paper offers a different, more accurate sensor calibration method. Moreover, this work offers experimental results for multiple sensors, ranges in the order of 250 m with ultra low-cost, portable SDR (that costs 7 Euro), while scalability issues are further examined.

A. Scatter Radio Principles

Scatter radio communication, known from 1948 [22], is currently exploited in the radio frequency identification (RFID) industry. Communication is implemented with an antenna, a control circuit and a radio frequency (RF) switch between them. The switch alternatively terminates the tag/sensor antenna between (usually two) loads Z_1 and Z_2 (Fig. 2). The control circuit is responsible for the modulation operation. Tag/sensor antenna S_{11} parameter (i.e., reflection coefficient Γ), associated with each antenna terminating load, is modified when the antenna load is changed. The different termination loads offer different reflection coefficients, (Γ_1 and Γ_2) according to the following [23]–[27]:

$$\Gamma_{\text{i}} = \frac{Z_{\text{i}} - Z_{\text{a}}^*}{Z_{\text{i}} + Z_{\text{a}}}, \tag{1}$$

with $\text{i} = 1, 2$ and Z_{a} denoting the antenna impedance.

Therefore, amplitude and phase of the carrier signal - induced at the sensor antenna - are modulated and the signal is reflected (scattered) back towards a receiver. As a result, when a continuous wave (CW) with frequency F_{c} is incident on the sensor antenna, which is alternatively terminated between two loads at a rate F_{sw}, two new subcarrier frequencies appear in the spectrum (Fig. 2); their frequency values are given by [28]:

$$F_{\text{sub},1} = F_{\text{c}} + F_{\text{sw}}, \tag{2}$$

$$F_{\text{sub},2} = F_{\text{c}} - F_{\text{sw}}. \tag{3}$$

While scatter-radio principles have been restricted to communication ranges of up to a few meter [29]–[31], a novel scatter radio sensor network (WSN) for relative humidity (%RH) measurements was presented in [32]. That WSN consisted of low-power and low-cost analog designs of wireless transmitters (sensor nodes/tags) with scatter radio and extended communication ranges. Each tag employed bistatic semi-passive scatter radio principles [33]. In order to address the small communication range problem, the WSN utilized the bistatic topology (where the carrier emitter was placed in a different location from the reader) and semi-passive (i.e., battery-assisted) tags. The utilization of the bistatic topology is illustrated in Fig. 3. Using the above concepts, it was shown possible to implement large-scale networks, comprising of low-cost sensor/tags, a few emitters operating at the European RFID band ($865 - 868$ MHz) [34] and a single software-defined radio (SDR) receiver, detecting the backscattered signals.

This work describes the development of a bistatic scatter radio WSN, that measures soil moisture percentage (%SM) with analog, frequency modulation (FM) principles and ranges in the order of 250 meter. In sharp contrast to prior art, this work offers a) custom capacitive sensing, b) soil moisture sensing and networking of multiple sensors (with corroborating experimental results), c) reception with ultra-low cost software-defined radio (SDR) that costs only a few Euro and d) special modulation design that offers scatter radio modulation signals with 50% duty cycle; the latter will be shown to be important for signal-to-noise ratio improvements at the SDR receiver, as well as for network scalability purposes.

Section II offers the design and implementation of the scatter radio sensor circuit, multiple access capability and power consumption tradeoff. Section III offers the SDR receiver design, based on a 8-bit ultra-low cost SDR, Section IV describes the simple calibration procedure and Section V offers the experimental results, including a relevant network demonstration and bistatic range measurements. Finally, work is concluded in Section VI.

II. Sensors Design and Implementation

The design target of the tags is to produce voltage pulses of fundamental frequency that depends on the %SM value and control the rate with which the antenna termination loads are alternated. For this purpose, the circuit diagram of Fig. 4 was designed, consisting of a custom capacitive soil moisture sensor, the capacitance-to-frequency converter (C2F), the power supply circuit and the scatter radio front-end.

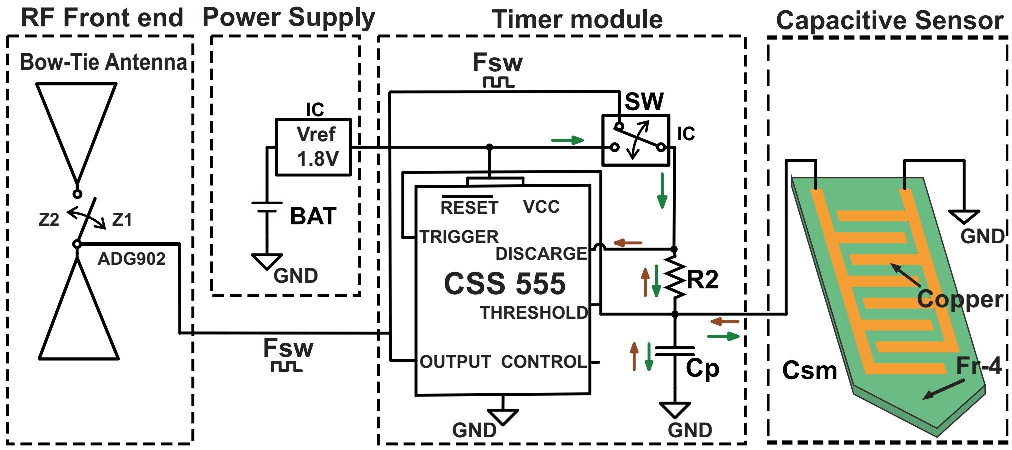

Fig. 4. The analog backscatter sensor node schematic. Each node consists of the capacitive soil moisture sensor to be inserted in the soil, the timer module that converts the variable capacitance to frequency (C2F) and the scatter radio front end. The variable frequency signal controls the antenna RF switch. The node is supplied by a voltage reference circuit.

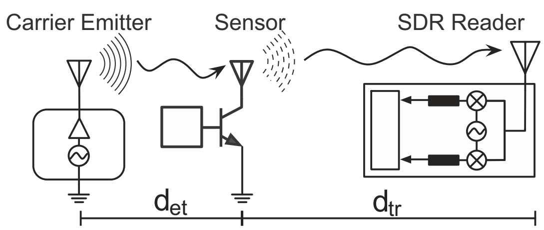

Fig. 3. Bistatic topology of a scatter radio link; emitter produces the carrier signal which is modulated by sensor nodes and finally, the reflected signal is received by a software defined radio (SDR) reader. $d_{\rm et}$ and $d_{\rm tr}$ denote emitter-to-tag and tag-to-reader distance, respectively. Notice that in this work, one emitter illuminates multiple tags, simultaneously.

A. Sensor & C2F Converter

A single astable multi-vibrator circuit with "555" timer functioned as the capacitance-to-frequency converter. The timer was the ultra low power monolithic CSS555 [35] with minimum current consumption of 5 uA at 1.2 V. The timer was connected to a resistor-capacitor network of R_2, $C_{\rm p}$ and to the custom, microstrip capacitive sensor $C_{\rm sm}$ (Fig. 4). The capacitive sensor consisted of two isolated conductive plates, separated by a narrow gap, on low cost FR-4 substrate with thickness 1.5 mm and and dielectric constant $\epsilon_{\rm r} = 4.6$; waterproofness was facilitated using the green solder mask as insulation. The followed capacitance sensor design is equivalent to a number of co-planar plate capacitors, inserted in parallel into the soil, which alters the dielectric constant; if soil is moist (high %SM), the capacitor will contain more water, resulting to higher capacitance (i.e., high $C_{\rm sm}$), while dry soil offers lower capacitance.

The fundamental frequency $F_{\rm sw}$ of the pulse depends on the resistor and the capacitor, connected to the TRIGGER and THRESHOLD pins of the "555" timer. As depicted in Fig. 4 (arrows), the parallel capacitors ($C_{\rm p}$ and $C_{\rm sm}$) are periodically charged and discharged through R_2 and an electronic, single-pole single-throw (SPST) switch (SW). The SW is open when timer output is in logic "low", so there is no leakage current through the SW loop and has been placed in order to reduce consumption, while attaining pulses with duty cycle of 50%; the latter is a fundamental difference compared to other capacitance-to-frequency converters in the literature (e.g., [32]). The timer output square wave pulse is offered with fundamental frequency given by:

$$F_{\rm sw} = \frac{1}{2\ln(2)R_2(C_{\rm p} + C_{\rm sm})}. \tag{4}$$

According to [36], the power of the fundamental subcarrier frequency of the scattered signal is given by:

$$P(a) = \left[\frac{A\sqrt{2}}{\pi}\sin(\pi D)\right]^2, \tag{5}$$

where A is the peak-to-peak amplitude of the pulse signal and D is the duty cycle; thus, the backscattered signal power will be increased when D approaches the value of 50%. Using a single analog switch (SW in Fig. 4) and only one resistor (R_2) in the typical astable multi-vibrator circuit, the duty cycle of the produced pulse is calculated as follows:

$$D = \frac{R_2}{2R_2} = 50\%. \tag{6}$$

According to its Fourier series analysis, a 50% duty-cycle square pulse consists of odd order harmonics of the fundamental frequency, i.e., even order harmonics are not present. Therefore, square waves without 50% duty-cycle occupy additional bandwidth, limiting the capacity of the designed network in a specific frequency band.

B. Scatter Radio Antenna/Front-end

The scatter radio front-end of each tag (Fig. 5, right bottom) consists of a microstrip bow-tie antenna on low-cost FR-4 substrate with an embedded RF switch; the latter is the Analog Devices ADG902 [37], set up as SPST switch. The ADG902 was chosen due to its low insertion loss (0.8 dB at 1 GHz) and high isolation (43 dB at 1 GHz). The front-end design was tuned around 868 MHz, according to the maximization principles in [27].

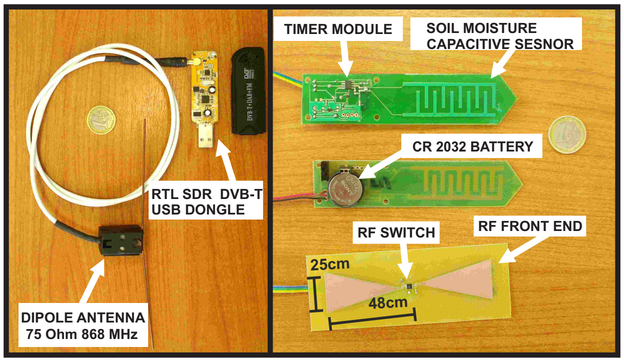

Fig. 5. The fabricated sensor node/tag (right). The green solder mask has been used as sensor insulation. Capacitive sensor and antenna/scatter radio front-end are fabricated on low-cost FR-4 substrate. The Realtek RTL software-defined radio (SDR) reader, depicted on the (left), is ultra-low cost on the order of 7 Euro.

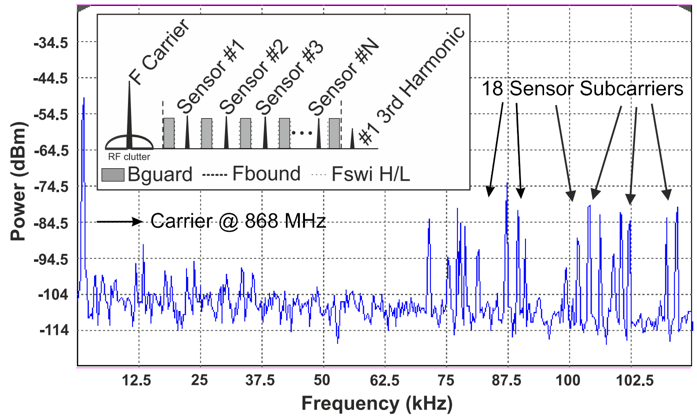

Fig. 6. Inlay figure with concept and frequency-division multiple access of simultaneously operating multiple tags; each tag operates in a different frequency band, while guard bands avoid adjacent-channel interference. *Measured* sensor network spectrum for sensors $\#1-18$.

A bowtie antenna for each sensor design was adopted, due to its omnidirectional attributes (at the vertical to its axe level) and the ease of fabrication, with nominal gain of $G = 1.8$ dBi. Fig. 5 offers dimensions. Such antenna is appropriate for the bistatic scatter radio topology, while a different printed antenna with higher gain could increase the ranging distance in the bistatic topology; however appropriate alignment during installation could be needed in that case.

C. Multiple Access

Simultaneous, collision-free operation of multiple, receiver-less sensors is facilitated with frequency-division multiple access principles [21], [28], [32]; every tag is assigned a distinct frequency band (bandwidth), within which the switching rate (i.e., subcarrier frequency) of each tag's antenna load can vary. Fig. 6 illustrates the concept with both conceptual and experimental data.

Let $F^{\mathrm{L}}_{\mathrm{sw,i}}$ and $F^{\mathrm{H}}_{\mathrm{sw,i}}$ denote the subcarrier frequency output of the i-th tag for lowest and highest frequency, produced by the C2F converter when the $\%$SM is 100 and 0, respectively. The required bandwidth B_{i} depends on the above two frequencies and is calculated as:

$$B_{\mathrm{i}} = F^{\mathrm{H}}_{\mathrm{sw,i}} - F^{\mathrm{L}}_{\mathrm{sw,i}}. \tag{7}$$

Assuming that C_{L}, C_{H} are the C_{sm} sensor capacitance for 0%, 100% SM, respectively, the $C_{\mathrm{p,i}}$ and $R_{2,\mathrm{i}}$ components of i-th tag are calculated according to (4), (7) as:

$$C_{\mathrm{p,i}} = \frac{-B_{\mathrm{i}}\ C_{\mathrm{L}} + F^{\mathrm{L}}_{\mathrm{sw,i}}\ (C_{\mathrm{H}} - C_{\mathrm{L}})}{B_{\mathrm{i}}}, \tag{8}$$

$$R_{2,\mathrm{i}} = \frac{B_{\mathrm{i}}}{2\ln(2)\ F^{\mathrm{L}}_{\mathrm{sw,i}}\ (C_{\mathrm{H}} - C_{\mathrm{L}})\ (F^{\mathrm{L}}_{\mathrm{sw,i}} + B_{\mathrm{i}})}. \tag{9}$$

It is noted that the outdoor environment temperature variations affect each sensor's circuit operation. For example, the CSS555 timer exhibits a temperature drift of 40 ppm/°C and thus, for a tag/sensor with nominal subcarrier frequency at 105 kHz, an extreme change of 30°C in temperature offers a frequency drift of $(40 * 30 * 105000)/10^6 = 126$ Hz. For bandwidth of 1.5 kHz per sensor, the aforementioned frequency shift amounts to $126/1500 = 8.4\%$ of each sensors bandwidth and a SM error in the same order. For ten times higher bandwidth per sensor, that drift would amount to only 0.84% error, with however reduced number of sensors in the available spectrum band. Thus, there is clearly a flexible tradeoff between scalability (in number of simultaneously operating sensors) and measurement accuracy.

For example, assuming operating (subcarrier) sensors' frequencies in 100 kHz-299 kHz, guard band of 1 kHz (to avoid adjacent-channel interference between sensors) and 1.5 kHz bandwidth/sensor, the capacity of the network results to 79 sensors. The upper limit of 299 kHz is selected in order to avoid the odd order harmonic of the lower limit subcarrier frequency of 100 kHz. Future work will install low-cost envelope detector receivers in each sensor, so that a subset of the sensors operate simultaneously and thus, the same number M of subcarrier frequencies is shared by a larger number N of sensors, where $N >> M$ (resembling GSM network architecture, where the same frequency channel is used by 8 users in TDMA mode).

D. Power Consumption & Tradeoff

The power supply circuit of each sensor is a crucial part, since its lifetime depends on it. For this purpose, a voltage reference integrated circuit (IC) and a coin battery were utilized. The power source was a 300 mAh, 3 V lithium-ion battery (type CR2032), connected with the C2F converter through the voltage reference component (Texas Instruments (TI) REF3318, [38]). The voltage reference consumed 5 uA only and supplied with stable voltage (V_{cc}) the whole circuit.

The total power dissipation of each sensor is calculated below:

$$P_{\mathrm{sensor}} = P_{\mathrm{charge}} + P_{\mathrm{quiescent}}, \tag{10}$$

with P_{charge}, the average power required for charging the capacitors and $P_{\mathrm{quiescent}}$, the quiescent power dissipated by the timer and the voltage reference IC. The components that were utilized in the sensor design consumed quiescent power of

TABLE I
POWER CONSUMPTION EXAMPLE FOR TWO SENSOR NODES.

Sensor #	V_{cc} (V)	R_2 (kΩ)	F_{sw} (kHz)	P_{tot} (μW)	Life (months)
1	1.8	3.6	70	267.7	5.2
2	1.8	0.793	150	1152	0.44

$P_{\text{quiescent}}$ = 17.87 μW. Moreover, average charging power was calculated according to [32] as:

$$P_{\text{charge}} = \frac{V_{\text{cc}}^2}{6R_2 \ln(2)}. \tag{11}$$

It can be seen that average power during charging P_{charge} depends on the fundamental (subcarrier) frequency, through resistor R_2. Consumption and lifetime example of two sensors is offered in Table I, including the corresponding resistor values, center frequency value and V_{cc}. The lifetime is the duration of continuous (non-duty-cycled) operation with the utilization of the above battery. It is obvious that the lifetime of sensor $\#2$ is too short due to the increased subcarrier center frequency. Fig. 7 presents the simulated power consumption of sensors as a function of subcarrier frequency. It is observed that when the center frequency of tags is increased from 60 kHz to 180 kHz, the power consumption is also (non-linearly) increased, with maximum value in the order of a mWatt; such relatively small power can be accommodated from various ambient solar, kinetic [39] or even thermoelectric [40] sources.

Scatter radio communication also depends on the RF clutter, i.e., the increased noise power spectral density around the carrier frequency. RF clutter is created due to reflections from the surrounding environment, as well as emitter's inherent phase jitter and non-linearities. Therefore, it is desirable for tags to operate as far as possible from the emitter's carrier frequency (i.e., as high as possible F_{sw}) in order to avoid increased noise power and hence, reduced signal-to-noise ratio. However, increased subcarrier frequency also increases power consumption and thus, reduces sensor's lifetime.

III. ULTRA-LOW COST WSN RECEIVER

One of the most important components of the scatter radio WSN is the receiver of the backscattered signals. The receiver is responsible for the fundamental frequency estimation of the incoming scattered subcarrier signals. In this work, the ultra-low cost Realtek (RTL) software-defined radio (SDR) was employed, that uses a DVB-T TV tuner dongle based on the RTL2832U chip (Fig. 5, left). It consists of an RF front-end and the Rafael Micro R820T tuner with frequency band range of 24-1766 MHz. The small cost on the order of a few Euro comes at the price of low dynamic range, since RTL offers only 8-bit resolution analog-to-digital converted (ADC) samples, pushed to a host computer through USB. Processing of the in-phase and quadrature signals (I/Q) is done solely in software at the host computer. A dipole 75 Ohm antenna was also designed to operate around 868 MHz. After a miniature coax connector for the antenna, there is a low noise amplifier (LNA) with noise figure (NF) of about 3.5 dB.

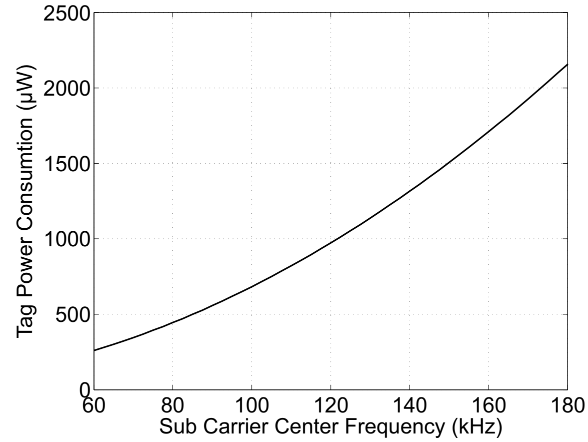

Fig. 7. Total power consumption versus sensor subcarrier frequency.

The fundamental subcarrier frequency $\hat{F}_{\text{i}}$ of the i-th sensor was estimated using the periodogram technique, which in turn is grounded on maximum likelihood principles. The estimated subcarrier was given according to:

$$\hat{F}_{\text{i}} = \underset{F \in [F_{\text{sw,i}}^{\text{L}}, F_{\text{sw,i}}^{\text{H}}]}{\arg\max} |X(F)|^2, \tag{12}$$

where $X(F)$ is the Fourier transform of the baseband down-converted and carrier frequency offset (CFO)-compensated signal. CFO estimation and compensation was based on standard periodogram techniques [41]. $F_{\text{sw,i}}^{\text{L}}$ and $F_{\text{sw,i}}^{\text{H}}$ mark the a-priori known lowest and highest possible frequency output of the i-th tag. Thus, the frequency component with the maximum power at each spectrum band is estimated as the corresponding sensor's output frequency.

IV. CALIBRATION

Deviations from nominal values of each tag's components (e.g., tolerance of capacitors, resistor or timer), as well as temperature dependence, require compensation, i.e., sensor calibration; the tags of this work were calibrated using polynomial surface fitting, utilizing both %SM and temperature parameter as input variables, as described below.

A soil sample was taken from the field, dried and filled a 1000 cubic centimetre (cc) container. Specific mass of water (in grams) was poured into the container and soil moisture percentage by volume was calculated, according to the following:

$$\text{Soil Moisture (\%) by Volume} = \frac{\text{Volume of Water}}{\text{Volume of Soil}} \times 100, \tag{13}$$

with

$$\text{Volume of Water} = \frac{\text{Mass of Water}}{\text{Density of Water}}, \tag{14}$$

with (well-known) density of water equal to 1 gram per cc.

Using the sensor design and the WSN reader described above, samples of subcarrier frequency were collected, for fixed temperature and variable soil moisture $\%$ (or vice

TABLE II
CALIBRATION FUNCTION AND FITTING ERROR.

Model	Fitted function	RMSE
3D	$f(x,y) = 105.5 + 0.232x + 0.0121y - 0.0074x^2$ $+0.0020xy - 0.0036y^2 + 7.531 * 10^{-5}x^3$ $-2.94 * 10^{-5}x^2y + 2.08 * 10^{-6}xy^2 + 3.65 * 10^{-5}y^3$	0.23 (kHz)

versa). Working with 226 sets of measurements (subcarrier frequency, temperature and soil moisture), minimum mean square error (MSE) cubic polynomial fitting was applied between subcarrier frequency, %SM and temperature. The outcome polynomial is given in Table II with corresponding fitting root mean squared error (RMSE). The surface (3D) transfer function is shown in Fig. 8 and a special case for fixed temperature 18.4°C, (2D) transfer function is shown in Fig. 9.

Fig. 9 shows an interesting saturation effect (at the output frequency), when the soil moisture by volume reaches 48%. That is due to the hydraulic properties of all soil textures. Specifically, *"total pore space, expressed on a volumetric basis, ranges from 40% in sandy soil to 48% in clay soil. When a soil is completely saturated, all the pores are filled with water. Thus, porosity is also the water content at saturation, expressed as the volume of water per volume of soil."* [42, chapter 6 "Soils", p. 167]. Thus, the observed saturation above 48% of the sensor is clearly coherent with the physical phenomenon of water content in various soil textures and thus, an indirect indication that the sensor is working properly.

Measured %SM results using the above procedure of (13), (14) were compared with the sensor's output; for data of Fig. 9 (fixed temperature), root mean squared error (RMSE) of 0.15% SM and mean absolute error (MAE) of 0.13% SM were found. Such error will be denoted as *calibration error*, since it does not include the error due to scatter radio communication, studied below.

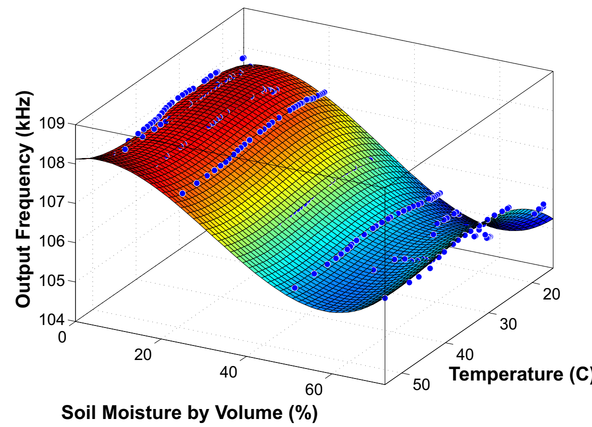

Fig. 8. Measured soil moisture (%) characteristic and polynomially-fitted function versus frequency and temperature for sensor #8. The data measurements were 226 sets of soil moisture, temperature and output frequency samples.

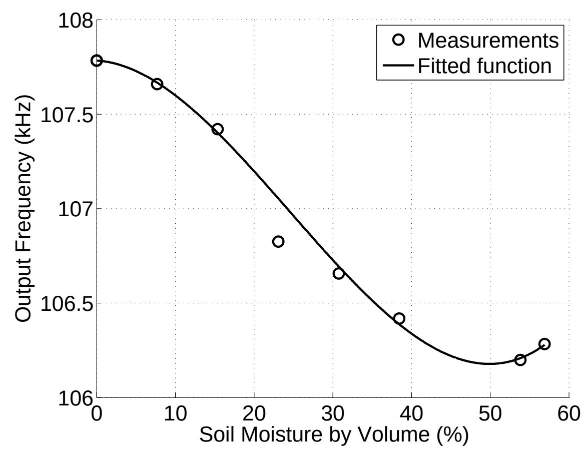

Fig. 9. Measured soil moisture (%) characteristic and fitted function versus frequency for sensor #8 for fixed environmental temperature (18.4°C).

V. EXPERIMENTAL RESULTS

Fig. 5 (right picture) depicts one of the fabricated sensor tags with low-cost FR-4 material and cost on the order of 6 Euro. At the installation site, each backscatter sensor node's bow-tie antenna (with its scatter radio front-end) was located well above the ground, while the fabricated capacitive sensor was inserted into the soil (Fig. 10) and the connection between those two parts was established with cables. The implemented demonstration WSN consisted of 18 scatter radio soil moisture sensors nodes, which could operate simultaneously, without collisions; Fig. 6 depicts the obtained sensors subcarriers and the emitter carrier at 868 MHz. Each sensor was allocated a unique 0.5 to 1.5 kHz frequency band (bandwidth) and there was a guard-band of 1 kHz between neighbouring-in-frequency tags to alleviate adjacent channel interference. Fig. 6 illustrates the subcarriers corresponding to 0% SM.

For demonstration purposes, a subset of the network was deployed in the indoor garden of Technical University of Crete. The bistatic topology scatter radio WSN with eight sensor nodes is depicted in Fig. 10. Carrier emitter (E) and RTL-SDR reader (R) were located at either sides of the field with the sensors in between. Capacitive sensors were inserted into the soil near the root of each plant, while the scatter radio front-ends were placed 1.5 meter above the ground, using canes.

Sampled data time series collected from approximately seven hours of continuous monitoring are illustrated in Fig. 11. It can be easily observed that after the watering instances, the output frequency of the sensors changed instantly, while it settled after a limited amount of time.

In order to achieve both communication performance characterization and sensing accuracy of the proposed WSN, maximum communication range and end-to-end sensing accuracy were experimentally measured. Specifically, a complete bistatic topology link was utilized outdoors (Fig. 12).

Carrier emitter, SDR receiver and sensor/tag (with subcarrier center frequency at 109 kHz) were installed at 1.3 m height. Temperature of 18°C was measured, soil moisture was fixed at 0% SM (corresponding to 109 kHz subcarrier frequency for the specific sensor), sampling rate was set to

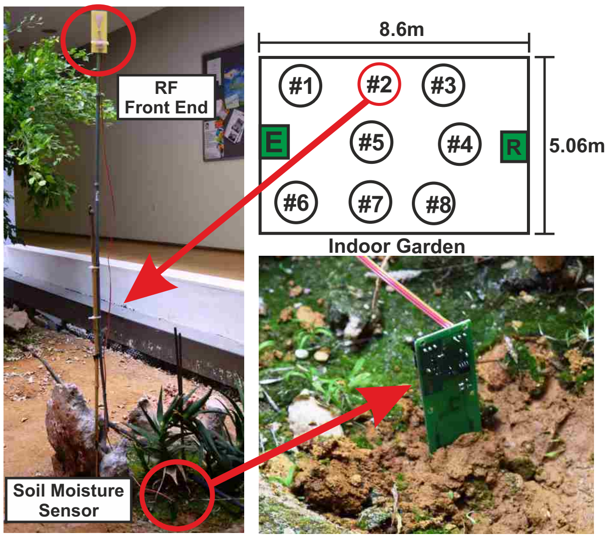

Fig. 10. Bistatic soil moisture sensor network demonstration; capacitive soil moisture sensor in installed into the ground, while scatter radio antenna is well above ground and being illuminated by the carrier emitter (E), while backscattered signal from various tags is received by the reader (R).

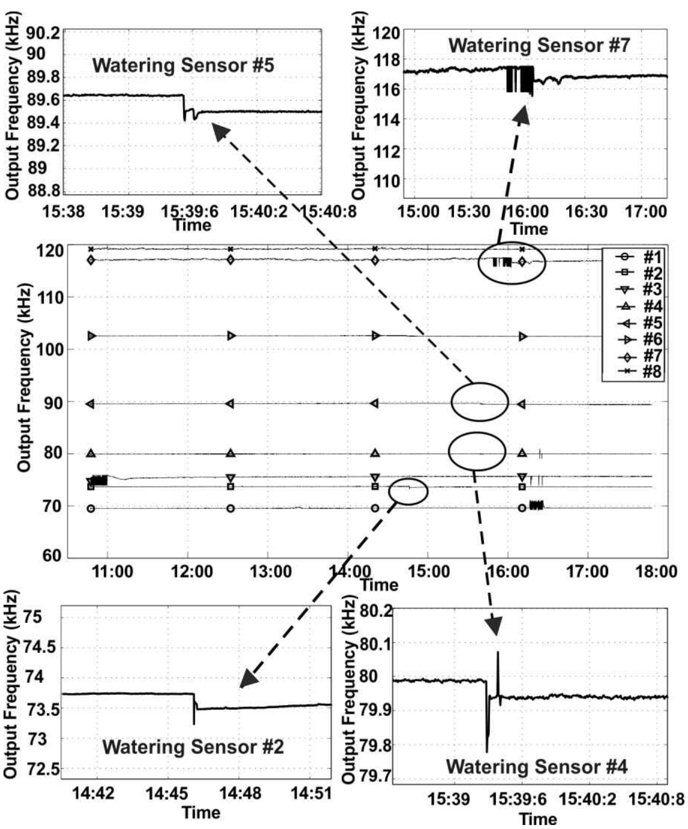

Fig. 11. Simultaneous and continuous soil moisture sensing from 8 tags, as a function of time, using the proposed scatter radio sensor network.

1 MHz and duration of 100 ms was exploited per sensor measurement. Communication performance was tested for various installation topologies and the corresponding results, in terms of estimating the transmitted subcarrier frequency, are presented in Table III, as a function of emitter-to-tag distance (d_{et}), tag-to-reader distance (d_{tr}) and root mean squared error

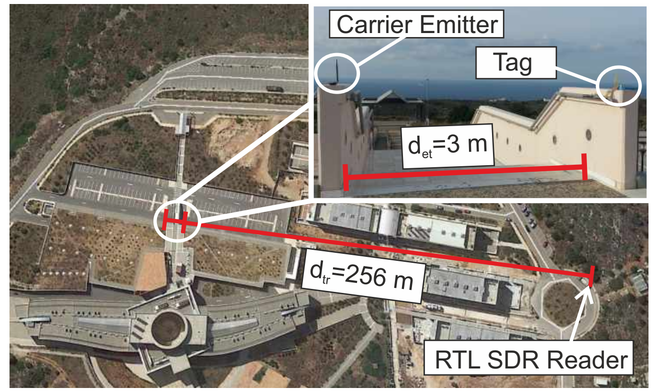

Fig. 12. Testing outdoors the communication range of the specific bistatic analog backscatter architecture.

TABLE III
Communication Accuracy.

#	d_{et} (m)	d_{tr} (m)	RMSE (Hz)	RMSE (%)
1	3	48.3	12.91	0.011
2	3	69	17.00	0.015
3	3	146	26.89	0.024
4	3	205	31.39	0.028
5	3	256	35.28	0.032
6	8.4	60.8	21.41	0.019
7	8.4	138	32.63	0.029
8	21.4	126	9.70	0.008

(RMSE) in Hz, after 1000 measurements, for each case (row) of Table III. Reference subcarrier value was measured with carrier emitter and SDR receiver in closed proximity with the sensor (and all the rest of the parameters the same), using average value out of 1000 sensor measurements.

Sensor-receiver ranges in the order of 256 meter are possible, with limited RMSE error in the order of 0.1%, due to wireless communication. Such small *communication error* suggests that communication ranges could be further increased and scatter radio communication range is not an issue. A similar finding, based on proper designs for scatter radio reception, has been also recently reported in [43]–[45]. Therefore, the overall sensor error is upper bounded by the sum of the RMSE calibration and communication errors under mild assumptions (e.g., independence of noise in sensor and and noise in receiver, unbiased errors etc.), which for the above values of Table III and the results of Section IV offers overall RMSE below 1% SM. Finally, it is noted that for all experimental results, emitter transmission power was 13 dBm at 868 MHz.

VI. Conclusion

This work described in detail the development of a scatter radio network of low-power and low-cost sensors of soil moisture. Communication ranges in the order of 250 meter were experimentally demonstrated, with overall RMSE, less than 1%. Scaling issues were also discussed. The low power consumption of each scatter radio sensor, in the order of 200 microWatts, enables powering from ambient energy sources (including RF and thermoelectric), left for future work.

Acknowledgment

The authors would like to thank all members of Telecom Fab Laboratory, School of Electronic and Computer Engineering, Technical University of Crete, and especially G. Vougioukas and K. Tzedaki for their help in various steps throughout this work.

References

[1] G. Vellidis, V. Garrick, S. Pocknee, C. Perry, C. Kvien, and M. Tucker, "How wireless will change agriculture," *Precision agriculture*, vol. 7, pp. 57–68, 2007.

[2] M. Haefke, S. Mukhopadhyay, and H. Ewald, "A Zigbee based smart sensing platform for monitoring environmental parameters," in *Proc. IEEE Int. Conf. on Instrum. and Meas. Techn. (I2MTC)*, Binjiang, China, May. 2011, pp. 1–8.

[3] G. R. Mendez, M. A. M. Yunus, and S. C. Mukhopadhyay, "A WiFi based smart wireless sensor network for monitoring an agricultural environment," in *Proc. IEEE Int. Conf. on Instrum. and Meas. Techn. (I2MTC)*, Graz, Austria, May. 2012, pp. 2640–2645.

[4] D. Antolín, A. Bayo, N. Medrano, B. Calvo, and S. Celma, "Wubinet: A flexible WSN for applications in environmental monitoring," in *Proc. IEEE Int. Conf. on Instrum. and Meas. Techn. (I2MTC)*, Graz, Austria, May. 2012, pp. 2608–2611.

[5] V. Palazzari, P. Mezzanotte, F. Alimenti, F. Fratini, G. Orecchini, M. Virili, C. Mariotti, and L. Roselli, "Leaf compatible "eco-friendly" temperature sensor clip for high density monitoring wireless networks," in *Proc. IEEE 15th Medit. Microw. Symp. (MMS)*, Lecce, Italy, Dec. 2015, pp. 1–4.

[6] Y. Kawahara, H. Lee, and M. M. Tentzeris, "Sensprout: inkjet-printed soil moisture and leaf wetness sensor," in *Proc. ACM Conf. on Ubiquitous Computing*, Pittsburgh, PA, Sep. 2012, pp. 545–545.

[7] S. Sulaiman, A. Manut, and A. Nur Firdaus, "Design, fabrication and testing of fringing electric field soil moisture sensor for wireless precision agriculture applications," in *Proc. IEEE Int. Conf. on Inf. and Multim. Techn. (ICIMT)*, Jeju Island, South Korea, Sep. 2009, pp. 513–516.

[8] S. Kim, Y. Kawahara, A. Georgiadis, A. Collado, and M. Tentzeris, "Low-cost inkjet-printed fully passive RFID tags using metamaterial-inspired antennas for capacitive sensing applications," in *Proc. IEEE Int. Microw. Symp. (IMS)*, Seattle, WA, Jun. 2013, pp. 1–4.

[9] Y. Liu, Y. He, M. Li, J. Wang, K. Liu, L. Mo, W. Dong, Z. Yang, M. Xi, J. Zhao, and X.-Y. Li, "Does wireless sensor network scale? A measurement study on GreenOrbs," in *Proc. IEEE INFOCOM*, Shanghai, China, Apr. 2011, pp. 873–881.

[10] S. Kim, C. Mariotti, F. Alimenti, P. Mezzanotte, A. Georgiadis, A. Collado, L. Roselli, and M. M. Tentzeris, "No battery required: perpetual RFID-enabled wireless sensors for cognitive intelligence applications," *IEEE Microw. Mag.*, vol. 14, no. 5, pp. 66–77, Jul. 2013.

[11] S. D. Assimonis, S.-N. Daskalakis, and A. Bletsas, "Sensitive and efficient RF harvesting supply for batteryless backscatter sensor networks," *IEEE Trans. Microw. Theory Techn.*, vol. 64, no. 4, pp. 1327–1338, Apr. 2016.

[12] J. Kimionis and M. M. Tentzeris, "RF tag front-end design for uncompromised communication and harvesting," in *Proc. IEEE Conf. on RFID Techn. and Appl. (RFID-TA)*, Tampere, Finland, Sep. 2014, pp. 109–114.

[13] S. D. Assimonis and A. Bletsas, "Energy harvesting with a low-cost and high efficiency rectenna for low-power input," in *Proc. IEEE Radio and Wireless Symp. (RWS)*, Newport Beach CA, USA, Jan. 2014, pp. 229–231.

[14] S. D. Assimonis, S.-N. Daskalakis, and A. Bletsas, "Efficient RF harvesting for low-power input with low-cost lossy substrate rectenna grid," in *Proc. IEEE Conf. on RFID Techn. and Appl. (RFID-TA)*, Tampere, Finland, Sep. 2014, pp. 1–6.

[15] K. Niotaki, F. Giuppi, A. Georgiadis, and A. Collado, "Solar/EM energy harvester for autonomous operation of a monitoring sensor platform," *Wireless Power Transfer*, vol. 1, no. 01, pp. 44–50, Mar. 2014.

[16] S. Caizzone, E. Digiampaolo, and G. Marrocco, "Investigation of suitable parameters for setup-independent RFID sensing," in *Proc. IEEE Int. EURASIP Workshop on RFID Techn. (EURFID)*, Rosenheim, Germany, Oct. 2015, pp. 98–102.

[17] C. Occhiuzzi, C. Paggi, and G. Marrocco, "Passive RFID strain-sensor based on meander-line antennas," *IEEE Antennas Propag. Mag.*, vol. 59, no. 12, pp. 4836–4840, Dec. 2011.

[18] R. Nair, E. Perret, S. Tedjini, and T. Barron, "A humidity sensor for passive chipless RFID applications," in *Proc. IEEE Conf. on RFID Techn. and Appl. (RFID-TA)*, Nice, France, Sep. 2012, pp. 29–33.

[19] R. Nair, E. Perret, and S. Tedjini, "Chipless RFID based on group delay encoding," in *Proc. IEEE Conf. on RFID Techn. and Appl. (RFID-TA)*, Sitges, Spain, Sep. 2011, pp. 214–218.

[20] S.-N. Daskalakis, S. D. Assimonis, E. Kampianakis, and A. Bletsas, "Soil moisture wireless sensing with analog scatter radio, low power, ultra-low cost and extended communication ranges," in *Proc. IEEE Sensors Conf.*, Valencia, Spain, Nov. 2014, pp. 122–125.

[21] A. Bletsas, S. Siachalou, and J. Sahalos, "Anti-collision tags for backscatter sensor networks," in *Proc. IEEE 38th Europ. Microw. Conf. (EuMC)*, Amsterdam, Netherlands, Oct. 2008, pp. 179–182.

[22] H. Stockman, "Communication by means of reflected power," *Proc. IEEE IRE*, pp. 1196–1204, Oct. 1948.

[23] K. Kurokawa, "Power waves and the scattering matrix," *IEEE Trans. Microw. Theory Techn.*, vol. 13, no. 2, pp. 194–202, Mar. 1965.

[24] P. V. Nikitin, K. S. Rao, S. F. Lam, V. Pillai, R. Martinez, and H. Heinrich, "Power reflection coefficient analysis for complex impedances in RFID tag design," *IEEE Trans. Microw. Theory Techn.*, vol. 53, no. 9, pp. 2721–2725, Sep. 2005.

[25] J. D. Griffin and G. D. Durgin, "Complete link budgets for backscatter-radio and RFID systems," *IEEE Antennas Propag. Mag.*, vol. 51, no. 2, pp. 11–25, Apr. 2009.

[26] A. Bletsas, A. G. Dimitriou, and J. N. Sahalos, "Improving backscatter radio tag efficiency," *IEEE Trans. Microw. Theory Techn.*, vol. 58, no. 6, pp. 1502–1509, Jun. 2010.

[27] S. D. Assimonis, E. Kampianakis, and A. Bletsas, "Microwave analysis and experimentation for improved backscatter radio," in *Proc. IEEE Europ. Conf. on Ant. and Prop. (EuCAP)*, Hague, Netherlands, Apr. 2014, pp. 3228–3229.

[28] G. Vannucci, A. Bletsas, and D. Leigh, "A software-defined radio system for backscatter sensor networks," *IEEE Trans. Wireless Commun.*, vol. 7, no. 6, pp. 2170–2179, Jun. 2008.

[29] S. Naderiparizi, A. N. Parks, Z. Kapetanovic, B. Ransford, and J. R. Smith, "Wispcam: A battery-free RFID camera," in *Proc. IEEE Int. Conf. on RFID*, Apr. 2015.

[30] Y. Zhao and J. R. Smith, "A battery-free RFID-based indoor acoustic localization platform," in *Proc. IEEE Int. Conf. on RFID*, Apr.–May 2013, pp. 110–117.

[31] A. Dementyev and J. R. Smith, "A wearable UHF RFID-based EEG system," in *Proc. IEEE Int. Conf. on RFID*, Apr.–May 2013, pp. 1–7.

[32] E. Kampianakis, J. Kimionis, K. Tountas, C. Konstantopoulos, E. Koutroulis, and A. Bletsas, "Wireless environmental sensor networking with analog scatter radio and timer principles," *IEEE Sensors J.*, vol. 14, no. 10, pp. 3365–3376, Oct. 2014.

[33] J. Kimionis, A. Bletsas, and J. N. Sahalos, "Bistatic backscatter radio for tag read-range extension," in *Proc. IEEE Conf. on RFID Techn. and Appl. (RFID-TA)*, Nice, France, Nov. 2012, pp. 356–361.

[34] ERC Rep. 25, 2015. [Online]. Available: http://www.erodocdb.dk/docs/doc98/official/pdf/ERCRep025.pdf

[35] *Custom Silicon Solutions, 2009*, CSS555 micropower timer, Product manual. [Online]. Available: http://www.customsiliconsolutions.com/downloads/Revised%20Standard%20products/CSS555_Spec.pdf

[36] S. W. Smith, *The scientist and engineer's guide to digital signal processing*. California Technical Publishing, San Diego, 1997.

[37] *Analog Devices (2005).*, ADG902 RF switch, Product manual. [Online]. Available: http://www.analog.com/media/en/technical-documentation/data-sheets/ADG901_902.pdf

[38] *Texas Instruments, (2014).* REF3318 voltage reference IC, Product manual. [Online]. Available: http://www.ti.com/lit/ds/symlink/ref3318.pdf

[39] *Perpetuum Inc. (2010).* Free-Standing Vibration Energy Harvester. [Online]. Available: http://www.perpetuum.com/fsh.asp

[40] *MicroPelt Inc. (2002).*, MPG-D651 Thermogenerator, Product manual. [Online]. Available: http://thermalforce.de/engl/product/thermogenerator/micropelt_d751.pdf

[41] P. Stoica and R. Moses, *Spectral Analysis of Signals*. Prentice-Hall International, Inc., 2005.

[42] G. B. Bonan, *Ecological climatology: Concepts and Applications, (1st edition)*. Cambridge Univ. Press, 2002.

[43] J. Kimionis, A. Bletsas, and J. N. Sahalos, "Increased range bistatic scatter radio," *IEEE Trans. Commun.*, vol. 62, no. 3, pp. 1091–1104, Mar. 2014.

[44] N. Fasarakis-Hilliard, P. Alevizos, and A. Bletsas, “Coherent detection and channel coding for bistatic scatter radio sensor networking,” *IEEE Trans. Commun.*, vol. 63, no. 5, pp. 1798–1810, May 2015.

[45] P. N. Alevizos and A. Bletsas, “Noncoherent composite hypothesis testing receivers for extended range bistatic scatter radio WSNs,” in *Proc. IEEE Int. Conf. on Commun. (ICC)*, London, UK, Jun. 2015, pp. 4448–4453.

Spyridon-Nektarios Daskalakis was born in Heraklion, Greece, in 1991. He received with excellence his Engineering Diploma in Electronic and Computer Engineering from Technical University of Crete (TUC) in 2014, and he is currently working toward the M.Sc. degree in the same school.

His current research interests include low-cost wireless sensor networks and RF energy harvesting. Particularly he focuses on scatter radio networking, batteryless sensors, PCB design, low cost software defined radio, environmental sensing and RF energy harvesting. He has received fellowship award for his project Aristeos (olive fly detection and monitoring with wireless sensor network) by the Clinton Global Initiative University 2014, Phoenix Arizona USA and the Onassis Foundation graduate studies 2015/16 scholarship.

Stylianos D. Assimonis was born in Thessaloniki, Greece.He received the Diploma/M.Eng. and Ph.D. degrees in electrical and computer engineering from the Aristotle University of Thessaloniki, Thessaloniki, Greece, in 2005 and 2011, respectively.

From 2012 to 2015, he was with the School of Electronic and Computer Engineering, Technical University of Crete, Chania, Greece, and the Radiocommunication Laboratory, School of Physics, Aristotle University of Thessaloniki, Thessaloniki, Greece, working as a Postdoctoral Researcher. He is currently a Senior Research Fellow with Queens University Belfast, Belfast, United Kingdom. His research interests span electromagnetism, RF/microwave/millimeter wave technologies, antennas, metamaterials and wireless communications.

Dr. Assimonis was the recipient of the Postdoctoral Scholarship for Excellence from the Research Committee of Aristotle University of Thessaloniki, Thessaloniki, Greece, in 2012, as well as the corecipient of the Metamaterials 2013 Best Paper Award (3rd place), the 2014 IEEE RFID-TA Best Student Paper competition finalist and the 2015 5th COST IC1301Workshop Best Student Paper award (3rd prize).

Eleftherios (Lefteris) Kampianakis received the Engineering Diploma and the M.Sc. in electronic and computer engineering from the Technical University of Crete, Chania, Greece, in 2011 and 2013 respectively. As an Undergraduate Researcher, he developed over the air programmed WSN testbeds with low-power software defined radio transceivers while his work as a Graduate Researcher during his M.Sc. regarded low-power, low-cost, and large-scale scatter radio WSN. He has received a fellowship award for his graduate studies, and was also a recipient of the Best Diploma Thesis Award-IEEE Vehicular Technology Society and Aerospace and Electronic Systems Society's Joint Greece Chapter Final/Diploma Thesis Competition. Currently he is a Ph.D. student at University of Washington, where he is developing implant systems for spinal cord injury treatment.

Aggelos Bletsas (S'03-M'05-SM'14) received the Diploma degree (with honors) in electrical and computer engineering from the Aristotle University of Thessaloniki (AUTh), Greece in 1998, and the S.M. and Ph.D. degrees from the Massachusetts Institute of Technology (MIT), Cambridge, MA, USA, in 2001 and 2005, respectively.

He was with Mitsubishi Electric Research Laboratories (MERL), Cambridge, MA, USA, as a Postdoctoral Fellow and with Radiocommunications Laboratory, Department of Physics, Aristotle University of Thessaloniki (AUTh), Greece, as a Visiting Scientist. He joined the School of Electronic and Computer Engineering, Technical University of Crete, Chania, Greece, in the summer of 2009, as an Assistant Professor and was promoted to Associate Professor at the beginning of 2014. He holds two patents from USPTO. His research interests span the broad area of scalable wireless communication and networking, with emphasis on relay techniques, backscatter communications and RFID, energy harvesting, radio hardware/software implementations for wireless transceivers, and low-cost sensor networks. His current vision and focus is on single-transistor front-ends and backscatter sensor networks, for large-scale environmental sensing. He is the Principal Investigator (PI) of project BLASE: Backscatter Sensor Networks for Large-Scale Environmental Sensing, funded from the General Secretariat of Research & Technology Action *"Proposals evaluated positively from the 3rd European Research Council (ERC) Call"*.

He is Management Committee (MC) member and National Representative in the European Union COST Action IC1301 *"Wireless Power Transmission for Sustainable Electronics (WIPE)"*. He has been an associate editor of the IEEE WIRELESS COMMUNICATION LETTERS since its foundation, an associate editor of the IEEE TRANSACTIONS ON WIRELESS COMMUNICATIONS and Technical Program Committee (TPC) member of flagship IEEE conferences.

Dr. Bletsas was the co-recipient of IEEE Communications Society 2008 Marconi Prize Paper Award in Wireless Communications, Best Paper distinction at ISWCS 2009, Siena, Italy, Second Best Student Paper Award at IEEE RFID-TA 2011, Sitges, Barcelona, Spain, Best Paper distinction at the IEEE Sensors Conf. (SENSORS), November 2013, Baltimore, MD, USA and Best Student Paper award at IEEE ICASSP 2015, April 2015, Brisbane, Australia. Two of his undergraduate advisees were winners of the 20092011 and 20112012 best Diploma Thesis contest, respectively, among all Greek Universities on "Advanced Wireless Systems", awarded by IEEE VTS/AES joint Greek Chapter. In 2013, he was the recipient of the Technical University of Crete 2013 Research Excellence Award.